

Article

Synthesis and Reactivities of Triphenyl Acetamide Analogs for Potential Nonlinear Optical Material Uses

Hira Israr ¹, Nasir Rasool ^{1,*}, Komal Rizwan ^{1,2}, Muhammad Ali Hashmi ^{3,4} , Tariq Mahmood ⁵, Umer Rashid ^{6,*} , Mohd Zobir Hussein ⁶  and Muhammad Nadeem Akhtar ⁷

¹ Department of Chemistry, Government College University, Faisalabad 38000, Pakistan; hiraisrar_gcuf@ymail.com (H.I.); komal.rizwan45@yahoo.com (K.R.)

² Department of Chemistry, Government College Women University, Faisalabad 38000, Pakistan

³ School of Chemical and Physical Sciences, Victoria University of Wellington, Wellington 6012, New Zealand; i4hashmi@hotmail.com

⁴ Department of Chemistry, University of Education, Attock Campus, Attock 43600, Pakistan

⁵ Department of Chemistry, COMSATS University Islamabad, Abbottabad Campus, University Road, Tobe Camp, Abbottabad 22060, Pakistan; tmahmoodhej@gmail.com

⁶ Institute of Advanced Technology, Universiti Putra Malaysia, UPM Serdang 43400, Selangor, Malaysia; mzobir@upm.edu.my

⁷ Faculty of Industrial Sciences & Technology, Universiti Malaysia Pahang, Gambang 26300, Malaysia; nadeemupm@gmail.com

* Correspondence: nasirrasool@gcuf.edu.pk (N.R.); umer.rashid@upm.edu.my (U.R.);

Tel.: +92-332-7491790 (N.R.); +60-3-97697393 (U.R.); Fax: +92-41-9201032 (N.R.); +60-3-97697004 (U.R.)

Received: 19 February 2019; Accepted: 23 March 2019; Published: 3 May 2019



Abstract: We have synthesized aniline based amides (**3a–h**) via palladium catalyzed Suzuki cross coupling of *N*-(2,5-dibromophenyl) acetamide with different arylboronic acids in moderate to good yields. A variety of functional groups were well tolerated in reaction conditions. For exploring the possible applications as optoelectronic devices, the nonlinear optical (NLO) properties of all synthesized derivatives (**3a–h**) were investigated with the help of density functional theory (DFT) methods. The frontier molecular orbitals analysis and reactivity descriptors were investigated for exploring the reactivities.

Keywords: aniline; Suzuki coupling; density functional theory; reactivity; palladium; optical

1. Introduction

Mono-, bi-, and tri-aryl-substituted aniline derivatives have been widely used for the synthesis of dyes, pharmaceuticals, ferromagnetic materials, and especially organometallic complexes [1–3]. For decades, aniline complexes have been a focus in organometallics and catalysis, such as *N*-heterocyclic carbene ligands (NHC) and β -diketiminateligands [4–9]. Aniline derivatives have been reported to possess antithrombolytic, antimicrobial, antioxidant, antitumor activities [10–12]. The polyanilines are promising products for potential industrial applications, and these are used in electronics and optics due to their electrical conductivity and good environmental stability [13,14]. Aniline based azo-dyes are medicinally well known as antineoplasticsm [15], antidiabetics [16], antiseptics [17], antibacterial, and antitumor agents [17]. They are well known in a number of biological reactions, such as inhibition of DNA and RNA, synthesis of proteins, carcinogenesis, and nitrogen fixation [18]. Aniline derivatives are known to inhibit the viral replication of HIV, and this effect is caused by the binding of azo-dyes to both the protease and the reverse transcriptase of this virus [19]. The Suzuki cross-coupling reaction is remarkably attractive and beneficial for the formation of C-C bonds due to high functional group tolerance, favorable reaction conditions, and easy handling of non-hazardous

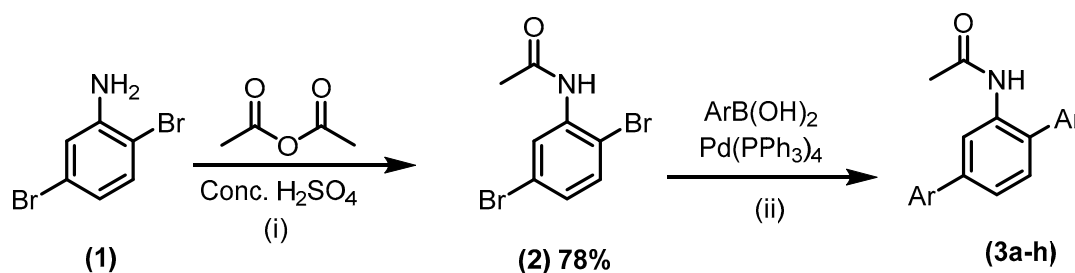
by-products [20–24]. In previous reports, the scientists have investigated and proposed that anilines possess good nonlinear optic (NLO) response and can have the potential to be used in different kinds of advance materials [25–27]. Keeping in view the importance of aniline derivatives, the present research was carried out to synthesize the various functionalized aniline derivatives via a palladium (Pd) catalyzed Suzuki coupling reaction. Furthermore, the first hyperpolarizability (β_0), which is directly related to the NLO response of any compound of all synthesized derivatives and frontier molecular orbitals (FMOs) analysis and reactivity descriptors, was calculated with the help of density functional calculations. To the best of our knowledge, all the studies reported in the current manuscript regarding aniline derivatives had not been reported in literature to date.

2. Results and Discussion

2.1. Chemistry

The protection of aromatic amino or hydroxyl groups in the form of amine derivatives or ethers and their subsequent cleavage constitute a useful chemical transformation in organic synthesis. In the present study, we investigated the Suzuki coupling of 2,5-dibromoaniline (**1**) with 3,5-difluoro and 3,5-dimethyl phenyl boronic acids, but no products were obtained. This reaction rendered unsuccessful because of the interference of an amino group on the benzene ring. This resulted in the failure of reactions that were performed without protection of the amino group. Later on, the revised method was carried out after the protection of the amino group. Herein, the current modification can be an attractive alternative to solve such problems.

Previously, our group reported the Suzuki coupling of 2-amino-6-bromobenzothiazole where low yields were obtained in a coupling reaction with an un-protected amino substrate, thus in order to obtain high yields, the amino group was protected via acylation, which led to substantially enhanced yields [28]. As presented in Scheme 1, in the first step, the amine group was protected by a reaction of 2,5-dibromoaniline (**1**) with acetic anhydride and intermediate protected *N*-(2,5-dibromophenyl)acetamide (**2**) was obtained in 78% yield.



Scheme 1. Conditions: *i*, **1** (1 g, 3.98 mmol), acetic anhydride (0.996 g, 9.96 mmol), H₂SO₄ (few drops), acetonitrile (10 mL), reflux. Conditions: *ii*, **2** (0.1 g, 0.341 mmol), Pd(PPh₃)₄ (0.019 g, 5 mol%), arylboronic acid (0.717 mmol), K₃PO₄ (0.2171 g, 1.024 mmol), 1,4-dioxane:H₂O (4:1 mL), reflux 32 h, 85–95 °C.

In the second step, Suzuki coupling of (**2**) with different arylboronic acids was conducted (Scheme 1), which eventually led to the synthesis of various tri-aryl acetamide derivatives (**3a–h**) in low to good yields (6–73%) (Figure 1). The triaryl compounds (**3a–h**) were obtained with the protected acetamide group. The compound **3a** showed high yield (73%) and **3h** showed 6% yield, while all other derivatives (**3d**, **3e**, **3c**, **3f**, **3b**, **3g**) showed moderate yields (43%, 40%, 38%, 37%, 34%, 33%), respectively. Different electron-donating and electron-withdrawing functional groups were well tolerated in the reaction, and they did not affect the reaction rate. Reaction conditions are responsible for the amount of product obtained. Moreover, the resulted group after protection was inert to all boronic acids, and it did not take part in any reaction. However, prolonged reaction time could de-protect that because of the basic medium.

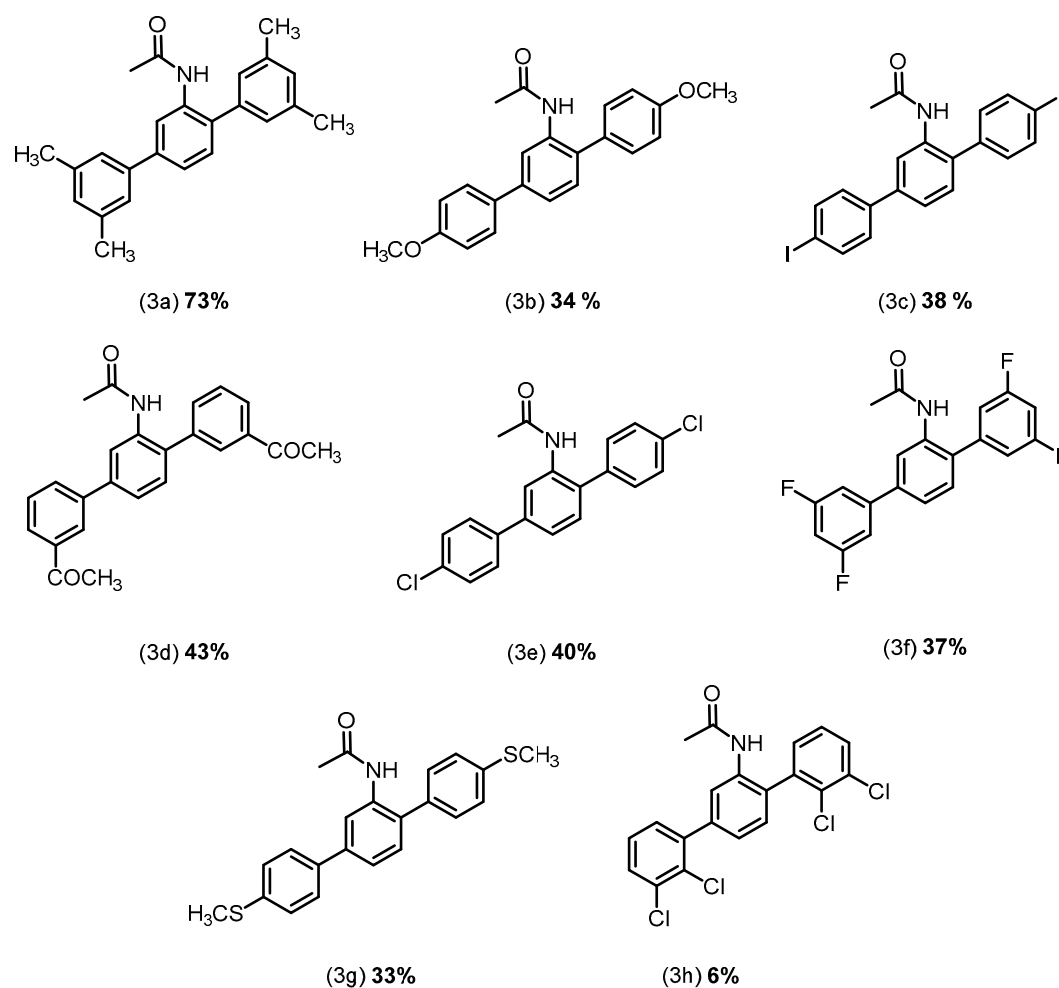


Figure 1. Suzuki coupling reaction of *N*-(2,5-dibromophenyl)acetamide (2) with different arylboronic acids.

It was noted that in the cases of products **3d** and **3g**, a mixture of mono- and di-arylated products was obtained in the Suzuki cross coupling reaction, and this may have been due to ineffective transmetallation and reductive elimination in the overall reaction cycle [29].

2.2. Computational Studies

2.2.1. Geometry Optimization

All the novel synthesized derivatives with different arylboronic acids (**3a–h**, Figure 2) were modeled in GaussView 5.0 and then optimized at the PBE0-D3BJ/def2-TZVP/SMD_{1,4}-dioxane level of theory using Gaussian 09. The optimized structures were confirmed to be true minima on the potential energy surface by confirming the absence of imaginary frequencies through the calculations of vibrational frequencies.

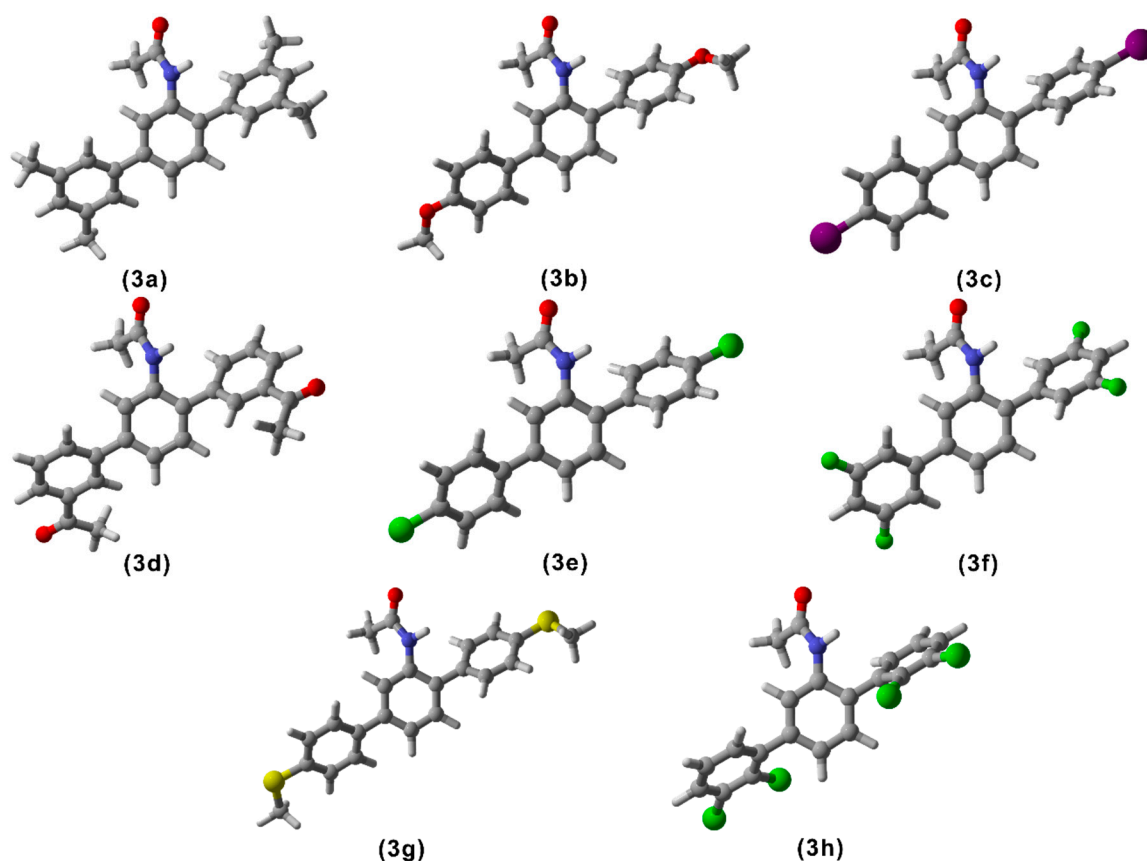


Figure 2. Optimized structures of all the aniline derivatives with different arylboronic acids (**3a–h**) at PBE0-D3BJ/def2-TZVP/SMD_{1,4}-dioxane level of theory.

In the 3D models, the grey color represents carbon, white represents hydrogens, green is for chlorine atoms, violet represents iodine atoms, red is for oxygen, yellow represents sulphur, and blue shows nitrogen atoms.

2.2.2. Frontier Molecular Orbital (FMO) Analysis

Due to the progressive development of the density functional theory (DFT), the calculation of frontier molecular orbitals of a molecule is fairly easy and provides insights into the electronic properties and reactivities of molecules [30]. The electronic transitions mainly occur between frontier orbitals (HOMO/LUMO), and their energy gap (HOMO-LUMO gap) can provide information about the reactivity and kinetic stability of the molecule [31]. The lower this energy gap is, the more reactive the compound is and vice versa. The FMO calculations were done at the same level of theory as the optimizations of the molecules, and plots of these orbitals are shown in Figure 3.

Table 1 represents the H-L_{Eg} values (ΔE) of all the compounds under study. These ΔE values of the molecules ranged from 4.51 to 5.32 eV. It was a narrow range, which indicated that, in general, the reactivity of these compounds was not much different. Compound **3g** had the lowest ΔE value (4.51 eV), which suggested it was the most reactive one in the series. Contrary to that, compound **3h** had the highest ΔE value, which made it the most stable in this series of compounds (**3a–h**).

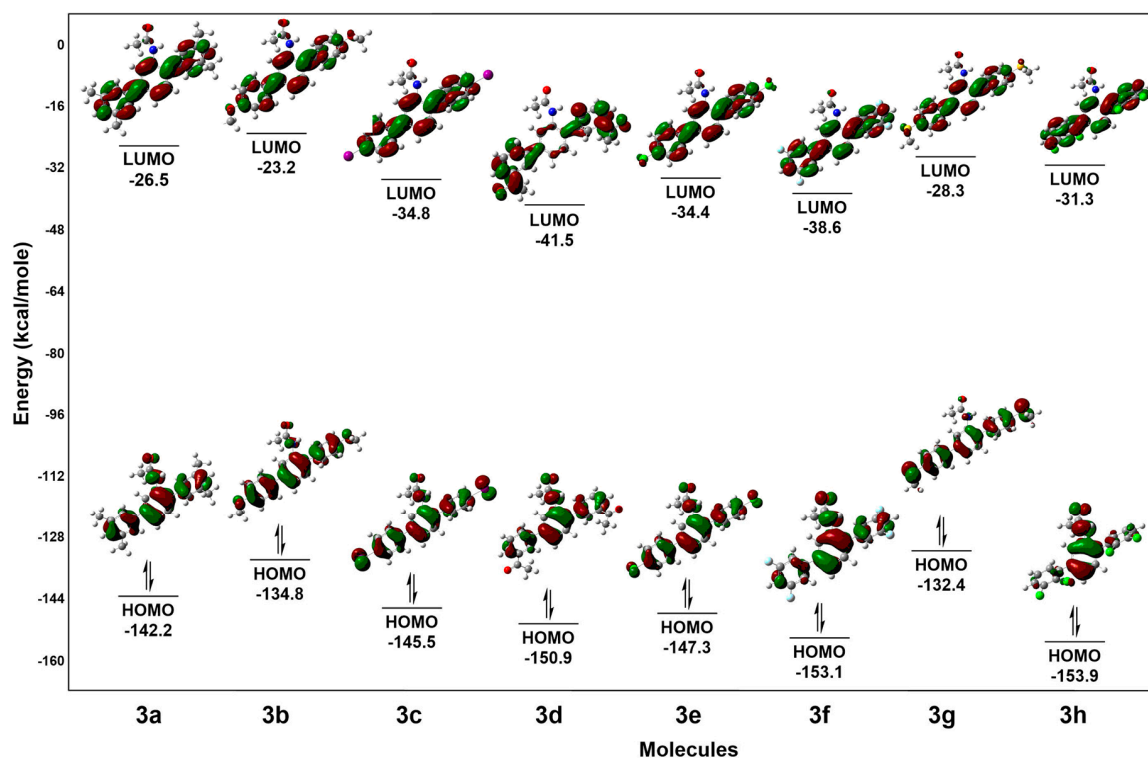


Figure 3. A plot of all the frontier orbitals of all the molecules (6a–6h) calculated at PBE0-D3BJ/def2-TZVP/SMD_{1,4}-dioxane level of theory.

Table 1. Energies of HOMO, LUMO, H-L_{Eg} and first hyperpolarizabilities (β_o) of all compounds (3a–h).

Compound	E_{HOMO} (eV)	E_{LUMO} (eV)	H-L _{Eg} (eV)	β_o (au)
3a	−6.17	−1.15	5.02	236.99
3b	−5.84	−1.01	4.84	465.20
3c	−6.31	−1.51	4.80	326.75
3d	−6.54	−1.80	4.75	775.01
3e	−6.39	−1.49	4.90	252.00
3f	−6.64	−1.67	4.96	311.90
3g	−5.74	−1.23	4.51	833.15
3h	−6.68	−1.36	5.32	245.70

The iso-density dispersion in the FMOs of these compounds showed quite similar trends for all of them except **3h**. The iso-density was mainly located on the phenyl rings for HOMO and LUMO, but in **3h**, the HOMO iso-density was found on the central phenyl ring and the acetamide group on it, while the LUMO iso-density was found on all the three phenyl rings, including the chlorine atoms. Having HOMO and LUMO distributed on such different functionalities made it the most stable compound. Compound **3g** was suggested to be the most reactive one with SMe groups on the phenyl rings. Here, the HOMO iso-density was found evenly distributed on all three phenyl rings and on both SMe groups. The less electro-negativity of sulphur and the electron-donating nature of SMe could explain this iso-density distribution, which showed a low HOMO-LUMO energy gap and rendered **3g** to be the most reactive in the series.

2.2.3. Nonlinear Optical Properties (NLO)

Materials with larger second-order NLO properties have been of considerable interest due to their potential applications in imaging technologies, optical computing, sensors, and medicinal applications [32–34]. The computed first hyperpolarizability (β_o) values of organic compounds

demonstrated their ability to support the movement of electrons. Higher β_o values showed greater push and pull of electrons with increased NLO response.

In the aniline derivatives in the present study (**3a–h**), the phenyl rings were acting as electron donors, while other present substituents acted as electron acceptors. Electron donating groups on phenyl rings increased the β_o values due to the increased movement of electrons. Contrary to that, the electron withdrawing groups made both ends electron acceptors, which in turn decreased the NLO response. In the present series of compounds, only compounds **3d** ($\beta_o = 775.01$ au) and **3g** ($\beta_o = 833.15$ au) showed a reasonably higher NLO response, as shown in Table 1. It was evident that the highest NLO response was shown by **3g**, which had two SMe groups on the *para* positions of the phenyl rings; **3e**, on the other hand, had two Cl atoms at the *para* positions and the lowest β_o value of 252.00 au due to its electron-withdrawing effect.

2.2.4. Conceptual Reactivity Descriptors

DFT can also give insights into other reactivity descriptors of compounds, which are important to explain the reactivity of a compound. These descriptors are given in Table 2 and were calculated according to Koopman's theorem, which says that the negative of E_{HOMO} and E_{LUMO} correspond to the ionization potential (I) and electron affinity (E_A) of the compound [35,36]. The other descriptors, i.e., chemical hardness (η), electronic chemical potential (μ), and electrophilicity index (ω), can then be computed as follows:

$$\eta = (E_{HOMO} - E_{LUMO})/2 \quad (1)$$

$$\mu = -(E_{HOMO} + E_{LUMO})/2 \quad (2)$$

$$\omega = \mu^2/2\eta \quad (3)$$

The values of all important reactivity descriptors of the compounds under study are given in Table 2.

Table 2. Reactivity indices of the compounds under study (**3a–h**).

Compound	Ionization Potential, I (eV)	Electron Affinity, (E_A) (eV)	Chemical Hardness, η (eV)	Electronic Chemical Potential, μ (eV)	Electrophilicity Index, ω (eV)
3a	6.17	1.15	2.51	−3.66	2.67
3b	5.84	1.01	2.42	−3.42	2.42
3c	6.31	1.51	2.40	−3.91	3.18
3d	6.54	1.80	2.37	−4.17	3.67
3e	6.39	1.49	2.45	−3.94	3.17
3f	6.64	1.67	2.48	−4.16	3.48
3g	5.74	1.23	2.26	−3.48	2.69
3h	6.68	1.36	2.66	−4.02	3.03

A detailed observation of Table 2 shows that different reactivity descriptors supported each other, thus strengthening the findings. According to the ΔE values discussed in the previous section, compound **3h** (Figure 3) was the most stable compound, which was supported by its highest ionization potential and chemical hardness values. Similarly, the most reactive compound—as predicted from FMO analysis—showed the lowest values of I , E_A , and η , thus supporting the predicted results.

3. Experimental

3.1. General

A melting point apparatus (B-540) was used for determining the melting points of synthesized solids. $^1\text{H-NMR}$ was measured using CDCl_3 (Bruker ARX, Billerica, MA, USA) at 300, 400, 500, 600 MHz). The JMS-HX-110 spectrometer with a data system was used for Electron Impact Mass

Spectrometry (EI-MS) spectra. Thin Layer Chromatography TLC was used for monitoring the completion of reaction (Merck silica gel 60 PF₂₅₄ cards).

3.2. General Procedure for the Synthesis of *N*-(2,5-Dibromophenyl)acetamide (**2**)

A solution of 2,5-dibromoaniline (**1**, 1 g, 3.98 mmol) and acetic anhydride (0.996 g, 9.96 mmol) in acetonitrile (10 mL) was stirred and refluxed at 60 °C with a few drops of 96% H₂SO₄ under an inert nitrogen atmosphere. The reaction was conducted for more than half an hour, and it was examined through TLC until completion. The volume of the reaction mixture was decreased by evaporating the solvent. Then, the solution was cooled to room temperature. Water was added drop wise to form precipitates. The mixture was stirred for one hour more at room temperature. After that, it was filtered. The work up was done by creating organic and aqueous layers and separating the organic layer. The solvent was evaporated through a rotary evaporator.

3.3. General Procedure for the Synthesis of Compound (**3a–h**)

N-(2,5-dibromophenyl)acetamide (**2**, 0.1 g, 0.341 mmol) and catalyst Pd(PPh₃)₄ (0.019 g, 5 mol%) were added in the schlenk flask with solvent 1,4-dioxane (8 mL). The reaction mixture was stirred for half an hour at room temperature. After that, arylboronic acid (0.717 mmol), K₃PO₄ (0.2171 g, 1.024 mmol), and water (2 mL) were added, and stirring and refluxing was done for 32 h at 85–95 °C. After cooling the reaction mixture to room temperature, it was filtered and diluted by solvent ethyl acetate. The work up was done by adding distilled water. Organic and aqueous layers were separated, and the organic layer was further processed. The solution was concentrated by rotary evaporation. The resulting sample was purified by column chromatography. The final product was dried, re-crystallized, and further analyzed by using different spectroscopic techniques.

3.4. Characterization Data

N-(2,5-Dibromophenyl)acetamide (**2**): solid, mp = 516 °C, ¹H-NMR (600 MHz, CDCl₃) δ: 8.57 (s, 1H, NH), 7.36 (d, *J* = 9.0 Hz, 1H, aryl), 7.09 (dd, *J* = 8.4, 1.8 Hz, 2H, aryl), 2.26 (s, 3H, CH₃). ¹³C-NMR (150 MHz, CDCl₃): δ 170.1, 142.0, 132.1, 130.1, 127.3, 122.4, 115.6, 24.0; EIMS (*m/z*, + ion mode): 293 [M + H]⁺; [M + 2] = 294.1; [M + 4] = 296.0; [M – Br]⁺ = 212.0.

N-(3,3',5,5'-Tetramethyl-[1,1':4',1''-terphenyl]-2'-yl)acetamide (**3a**): solid, mp = 680 °C, ¹H-NMR (600 MHz, CDCl₃) δ: 8.57 (s, 1H, NH), 7.36 (d, *J* = 8.4 Hz, 2H, aryl), 7.26–7.17 (m 3H, aryl), 7.04–6.98 (m, 4H, aryl), 2.26 (s, 12H, CH₃), 2.02 (s, 3H, CH₃). ¹³C-NMR (150 MHz, CDCl₃): δ 167.1, 140.1, 139.1, 138.9, 138.3, 137.9, 137.1, 136.1, 135.1, 129.1, 128.5, 128.1, 127.1, 126.3, 125.8, 125.1, 123.4, 122.8, 121.1, 25.0, 23.1, 22.3, 21.9, 21.1. EIMS (*m/z*, + ion mode): 343.3 [M + H]⁺, [M – Me]⁺ = 328.0.

N-(4,4'-Dimethoxy-[1,1':4',1''-terphenyl]-2'-yl)acetamide (**3b**): solid, mp = 677 °C, ¹H-NMR (600 MHz, CDCl₃) δ: 9.02 (s, 1H, NH), 8.01 (d, *J* = 7.8 Hz, 2H, aryl), 7.65–7.35 (m, 4H, aryl), 7.10 (d, *J* = 8.2 Hz, 2H, aryl), 7.04–7.02 (m, 3H, aryl), 2.42 (s, 6H, OCH₃), 2.32 (s, 3H, CH₃). ¹³C-NMR (150 MHz, CDCl₃): δ 170.1, 160.1, 159.1, 140.1, 138.1, 135.1, 134.1, 132.1, 131.1, 130.8, 131.1, 129.1, 124.1, 121.9, 120.1, 116.1, 115.8, 115.1, 114.0, 56.9, 55.1, 25.0 EIMS (*m/z*, + ion mode): 348.1 [M + H]⁺, [M – OMe]⁺ = 317.1, [M – 2OMe]⁺ = 286.4.

N-(4,4'-Diiodo-[1,1':4',1''-terphenyl]-2'-yl)acetamide (**3c**): solid, mp = 726 °C, ¹H-NMR (600 MHz, CDCl₃) δ: 9.05 (s, 1H, NH), 8.21 (d, *J* = 7.6 Hz, 2H, aryl), 7.81–7.77 (m, 4H, aryl), 7.57–7.52 (m, 5H, aryl), 2.23 (s, 3H, CH₃). ¹³C-NMR (150 MHz, CDCl₃): δ 170.1, 140.5, 139.7, 138.7, 138.1, 137.2, 136.6, 135.9, 134.1, 133.7, 132.1, 131.1, 129.1, 124.1, 123.7, 122.1, 120.1, 94.2, 93.4, 25.7. EIMS (*m/z*, + ion mode): 540.1 [M + H]⁺, [M – I]⁺ = 413.1, [M – 2I]⁺ = 285.9.

N-(3,3'-Diacetyl-[1,1':4',1''-terphenyl]-2'-yl)acetamide (**3d**): solid, mp = 755 °C, ¹H-NMR (600 MHz, CDCl₃) δ: 9.32 (s, 1H, NH), 8.01–7.91 (m, 3H, aryl), 7.65–7.35 (m, 6H, aryl), 6.87 (d, *J* = 3.5 Hz, 2H, aryl), 2.64 (s, 6H, COCH₃), 2.26 (s, 3H, CH₃). ¹³C-NMR (150 MHz, CDCl₃): δ 197.9, 197.1, 167.1, 142.3, 140.1,

139.1, 137.8, 137.1, 135.1, 132.1, 131.1, 128.9, 128.1, 127.6, 126.8, 126.1, 125.1, 121.7, 120.1, 27.1, 26.6, 23.1. EIMS (m/z , + ion mode): 372.2 $[M + H]^+$, $[M - COCH_3]^+ = 329.1$, $[M - 2COCH_3]^+ = 285.2$, $[M - aryl, COCH_3, fragments]^+ = 253.2$.

N-(4,4''-Dichloro-[1,1':4',1''-terphenyl]-2'-yl)acetamide (**3e**): solid, mp = 670 °C, 1H -NMR (600 MHz, $CDCl_3$) δ : 8.42 (s, 1H, NH), δ : 7.56 (d, $J = 10.0$ Hz, 2H, aryl), 7.46 (d, $J = 9.4$ Hz, 3H, aryl), 7.39 (d, $J = 8.5$ Hz, 3H, aryl), 7.35–7.31 (m, 3H, aryl), 2.02 (s, 3H, CH_3). ^{13}C -NMR (150 MHz, $CDCl_3$): δ 170.1, 140.1, 139.1, 138.8, 137.1, 132.6, 131.1, 130.7, 130.1, 129.4, 128.1, 127.6, 126.1, 125.3, 124.6, 124.0, 121.9, 121.1, 119.8, 23.9. EIMS (m/z , + ion mode): 355.0 $[M + H]^+$, 456.1 $[M + 2]$; 358.1 $[M + 4]$; $[M - Cl, NHCOCH_3]^+ = 262.0$, $[M - 2Cl, NHCOCH_3]^+ = 226.0$.

N-(3,3'',5,5''-Tetrafluoro-[1,1':4',1''-terphenyl]-2'-yl)acetamide (**3f**): solid, mp = 637 °C, 1H -NMR (600 MHz, $CDCl_3$) δ : 8.65 (s, 1H, NH), 7.85–7.81 (m, 4H, aryl), 7.65 (d, $J = 8.1$ Hz, 2H, aryl), 7.05–7.01 (m, 3H, aryl), 2.12 (s, 3H, CH_3). ^{13}C -NMR (150 MHz, $CDCl_3$): δ 170.1, 169.1, 168.1, 166.9, 165.2, 140.9, 139.8, 138.2, 137.1, 129.0, 125.7, 122.7, 120.3, 114.0, 113.7, 112.1, 111.0, 104.1, 103.5, 23.6. EIMS (m/z , + ion mode): 360.0 $[M + H]^+$, $[M - NHCOCH_3]^+ = 302.0$, $[M - 4F]^+ = 284.0$.

N-(4,4''-Bis(methylthio)-[1,1':4',1''-terphenyl]-2'-yl)acetamide (**3g**): solid, mp = 710 °C, 1H -NMR (600 MHz, $CDCl_3$) δ : 8.56 (s, 1H, NH), 7.83–7.80 (m, 4H, aryl), 7.77–7.73 (m, 3H, aryl), 7.36 (d, $J = 8.4$ Hz, 2H, aryl), 7.09 (dd, $J = 8.4, 2.4$ Hz, 2H, aryl), 2.23 (s, 6H, SCH_3), 2.01 (s, 3H, CH_3). ^{13}C -NMR (150 MHz, $CDCl_3$): δ 170.1, 139.7, 138.5, 137.3, 136.2, 135.6, 135.1, 130.9, 128.4, 127.1, 126.9, 126.1, 125.7, 125.0, 124.6, 123.6, 122.4, 120.4, 119.0, 25.8, 15.6, 15.0. EIMS (m/z , + ion mode): 380.0 $[M + H]^+$, $[M - NHCOCH_3]^+ = 321.0$, $[M - SCH_3, aryl fragments]^+ = 256.1$, $[M - NHCOCH_3, SCH_3, aryl fragments]^+ = 199.1$.

N-(2,2'',3,3''-Tetrachloro-[1,1':4',1''-terphenyl]-2'-yl)acetamide (**3h**): solid, mp = 754 °C, 1H -NMR (600 MHz, $CDCl_3$) δ : 8.95 (s, 1H, NH), 7.47 (d, $J = 7.8$ Hz, 2H, aryl), 7.30 (t, $J = 7.8$ Hz, 3H, aryl), 7.10–7.08 (m, 4H, aryl), 2.16 (s, 3H, CH_3). ^{13}C -NMR (150 MHz, $CDCl_3$): δ 171.0, 143.1, 140.1, 138.7, 137.1, 136.3, 135.2, 134.7, 132.0, 130.1, 128.9, 128.1, 127.4, 126.7, 125.9, 124.7, 123.7, 122.0, 121.8, 25.7. EIMS (m/z , + ion mode): 426.1 $[M + H]^+$, 427.1 $[M + 2]$; 429.1 $[M + 4]$; 431 $[M + 6]$, 433.7 $[M + 8]$, $[M - 2Cl, aryl fragments]^+ = 279.0$.

3.5. Computational Methods

Gaussian 09 (Revision D.01) [37] was used for all the calculations. The density functional theory (DFT) was employed for all the calculations, utilizing Adamo's hybrid [38] version of Perdew, Burke and Ernzerhof functional (PBE0) [39,40] along with the application of Grimme's empirical dispersion correction (D3) with Becke-Johnston damping (D3BJ) [41–43]. All the calculations were performed with Ahlrich's triplet ζ basis set Def2-TZVP [44] aided by the Polarizable Continuum Model (PCM) with the integral equation formalism variant (IEFPCM) [45–51] for solvation modeling. The solvent for all the calculations was 1,4-dioxane, which was modeled with the SMD parameter set by Cramer and Truhlar [52] (as implemented in Gaussian 09) [37]. All optimized structures were established to be true minima on the potential energy surface at the PBE0-D3BJ/def2-TZVP/SMD_{1,4-dioxane} level by calculating the vibrational frequencies with the absence of imaginary frequencies. NLO calculations were performed at the same level of theory as optimizations. The 3D images of optimized molecules were drawn using GaussView 5.0.9 and CYLview [53] programs.

4. Conclusions

A series of novel amides (**3a–h**) was synthesized via a Suzuki cross coupling reaction. The density functional theory calculations were performed on the synthesized aniline derivatives to gain insight into their structural and electronic properties. An analysis of the frontier orbitals and other reactivity descriptors, including ionization potential, electron affinity, chemical hardness, electronic chemical potential, and electrophilicity index, showed that compound **3g** was the most reactive one, while **3h** was the most stable one. The first hyperpolarizability (β_0) analysis revealed that **3g** (833.15 au) had a

reasonably high NLO response, whereas **3e** had the lowest β_0 value of 252.00 au among all synthesized derivatives. The NLO response revealed that in the future, these derivatives have potential applications in optoelectronic devices.

Author Contributions: For this research article, all authors have various contributions. Conceptualization, N.R.; methodology, H.I.; software, M.A.H. and T.M.; validation, K.R.; formal analysis, M.A.H. and T.M.; investigation, M.N.A.; resources, H.I.; writing—original draft preparation, K.R., T.M.; writing—review and editing, K.R.; visualization and supervision, N.R.; project administration, N.R.; analysis, writing—review and editing, U.R.; review and editing, results evaluation (M.Z.H.).

Funding: The authors gratefully acknowledge Government college University Faisalabad for financial support under research support program (GCUF-RSP) with Project # 73-CHM-13.

Conflicts of Interest: The authors declare no conflicts of interest.

References

1. Li, J.J.; Wang, H.; Tino, J.A.; Robl, J.A.; Herpin, T.F.; Lawrence, R.M.; Biller, S.; Jamil, H.; Ponticciello, R.; Chen, L.; et al. 2-Hydroxy-N-arylbenzenesulfonamides as ATP-citrate lyase inhibitors. *Bioorgan. Med. Chem. Lett.* **2007**, *17*, 3208–3211. [[CrossRef](#)]
2. Meinhard, D.; Wegner, M.; Kipiani, G.; Hearley, A.; Reuter, P.; Fischer, S.; Marti, O.; Rieger, B. New nickel (II) diimine complexes and the control of polyethylene microstructure by catalyst design. *J. Am. Chem. Soc.* **2007**, *129*, 9182–9191. [[CrossRef](#)] [[PubMed](#)]
3. Langhals, H.; Ismael, R.; Yürük, O. Persistent fluorescence of perylene dyes by steric inhibition of aggregation. *Tetrahedron* **2000**, *56*, 5435–5441. [[CrossRef](#)]
4. Zakai, U.I.; Bloch-Mechkour, A.; Jacobsen, N.E.; Abrell, L.; Lin, G.; Nichol, G.S.; Bally, T.; Glass, R.S. Synthesis and structure of m-terphenyl thio-, seleno-, and telluroethers. *J. Organ. Chem.* **2010**, *75*, 8363–8371. [[CrossRef](#)] [[PubMed](#)]
5. Zuideveld, M.A.; Wehrmann, P.; Röhr, C.; Mecking, S. Remote substituents controlling catalytic polymerization by very active and robust neutral nickel (II) complexes. *Angew. Chem.* **2004**, *116*, 887–891. [[CrossRef](#)]
6. Alexander, S.G.; Cole, M.L.; Morris, J.C. Preparation of a super bulky silver N-heterocyclic carbene complex. *New J. Chem.* **2009**, *33*, 720–724. [[CrossRef](#)]
7. Eberhardt, R.; Allmendinger, M.; Luinstra, G.A.; Rieger, B. The ethylsulfinate ligand: A highly efficient initiating group for the zinc β -diiminate catalyzed copolymerization reaction of CO₂ and epoxides. *Organometallics* **2003**, *22*, 211–214. [[CrossRef](#)]
8. Bai, G.; Singh, S.; Roesky, H.W.; Noltemeyer, M.; Schmidt, H.-G. Mononuclear aluminum hydroxide for the design of well-defined homogeneous catalysts. *J. Am. Chem. Soc.* **2005**, *127*, 3449–3455. [[CrossRef](#)] [[PubMed](#)]
9. Lee, D.-H.; Jin, M.-J. An extremely active and general catalyst for Suzuki coupling reaction of unreactive aryl chlorides. *Organ. Lett.* **2010**, *13*, 252–255. [[CrossRef](#)]
10. Iqbal, J.; Tirmizi, S.A.; Wattoo, F.H.; Imran, M.; Wattoo, M.H.S.; Sharfuddin, S.; Latif, S. Biological properties of chloro-salicylidene aniline and its complexes with Co (II) and Cu (II). *Turk. J. Biol.* **2006**, *30*, 1–4.
11. Gizdavic-Nikolaidis, M.R.; Bennett, J.R.; Swift, S.; Easteal, A.J.; Ambrose, M. Broad spectrum antimicrobial activity of functionalized polyanilines. *Acta Biomater.* **2011**, *7*, 4204–4209. [[CrossRef](#)] [[PubMed](#)]
12. Zhu, X.-K.; Guan, J.; Tachibana, Y.; Bastow, K.F.; Cho, S.J.; Cheng, H.-H.; Cheng, Y.-C.; Gurwith, M.; Lee, K.-H. Antitumor Agents. 194. Synthesis and biological evaluations of 4- β -mono-, -di-, and -trisubstituted aniline-4'-O-demethyl-podophyllotoxin and related compounds with improved pharmacological profiles. *J. Med. Chem.* **1999**, *42*, 2441–2446. [[CrossRef](#)]
13. Jangid, N.K.; Chauhan, N.P.S.; Meghwal, K.; Ameta, R.; Punjabi, P.B. Synthesis of dye-substituted polyanilines and study of their conducting and antimicrobial behavior. *Cogent Chem.* **2015**, *1*, 1084666. [[CrossRef](#)]
14. Yılmaz, K.; Akgoz, A.; Cabuk, M.; Karaagac, H.; Karabulut, O.; Yavuz, M. Electrical transport, optical and thermal properties of polyaniline–pumice composites. *Mater. Chem. Phys.* **2011**, *130*, 956–961. [[CrossRef](#)]
15. Child, R.; Wilkinson, R.; Tomcu-Fucik, A. Effect of Substrate orientation of the adhesion of polymer joints. *Chem. Abstr.* **1977**, *1977*, 6031.
16. Garg, H.; Prakash, C. Potential antidiabetics. 11. Preparation of 4-arylozo-3, 5-disubstituted-(2H)-1, 2, 6-thiadiazine 1, 1-dioxides. *J. Med. Chem.* **1972**, *15*, 435–436. [[CrossRef](#)]

17. Rathod, K.; Thakre, N. Synthesis and antimicrobial activity of azo compounds containing m-cresol moiety. *Chem. Sci. Trans.* **2013**, *2*, 25–28. [[CrossRef](#)]
18. Park, C.; Lim, J.-S.; Lee, Y.; Lee, B.; Kim, S.-W.; Lee, J.; Kim, S. Optimization and morphology for decolorization of reactive black 5 by *Funalia trogii*. *Enzyme Microb. Technol.* **2007**, *40*, 1758–1764. [[CrossRef](#)]
19. Swati, G.; Romila, K.; Sharma, I.; Verma, P. Synthesis, characterization and antimicrobial screening of some azo compounds. *Int. J. Appl. Biol. Pharm. Technol.* **2011**, *2*, 332–338.
20. Martin, A.R.; Yang, Y. Palladium-catalyzed cross-coupling reactions of organoboronic acids with organic electrophiles. *Acta Chem. Scand.* **1993**, *47*, 221–230. [[CrossRef](#)]
21. Suzuki, A. New synthetic transformations via organoboron compounds. *Pure Appl. Chem.* **1994**, *66*, 213–222. [[CrossRef](#)]
22. Stanforth, S.P. Catalytic cross-coupling reactions in biaryl synthesis. *Tetrahedron* **1998**, *54*, 263–303. [[CrossRef](#)]
23. Suzuki, A. Recent advances in the cross-coupling reactions of organoboron derivatives with organic electrophiles, 1995–1998. *J. Organomet. Chem.* **1999**, *576*, 147–168. [[CrossRef](#)]
24. Miyaura, N.; Suzuki, A. Palladium-catalyzed cross-coupling reactions of organoboron compounds. *Chem. Rev.* **1995**, *95*, 2457–2483. [[CrossRef](#)]
25. Shi, J.-M.; Xu, W.; Liu, Q.-Y.; Liu, F.-L.; Huang, Z.-L.; Lei, H.; Yu, W.-T.; Fang, Q. Polynitrile-bridged two-dimensional crystal: Eu (III) complex with strong fluorescence emission and NLO property. *Chem. Commun.* **2002**, *123*, 756–757. [[CrossRef](#)]
26. Chang, H.-L.; Lin, H.-L.; Wang, Y.-C.; Dai, S.A.; Su, W.-C.; Jeng, R.-J. Thermally stable NLO poly (amide-imide)s via sequential self-repetitive reaction. *Polymer* **2007**, *48*, 2046–2055. [[CrossRef](#)]
27. Kolev, T.; Koleva, B.B.; Spassov, T.; Cherneva, E.; Spitteller, M.; Mayer-Figge, H.; Sheldrick, W.S. Synthesis, spectroscopic, thermal and structural elucidation of 5-amino-2-methoxypyridine ester amide of squaric acid ethyl ester: A new material with an infinite pseudo-layered structure and manifested NLO application. *J. Mol. Struct.* **2008**, *875*, 372–381. [[CrossRef](#)]
28. Gull, Y.; Rasool, N.; Noreen, M.; Altaf, A.A.; Musharraf, S.G.; Zubair, M.; Nasim, F.-U.-H.; Yaqoob, A.; DeFeo, V.; Zia-Ul-Haq, M. Synthesis of N-(6-arylbenzo [d] thiazole-2-acetamide derivatives and their biological activities: An experimental and computational approach. *Molecules* **2016**, *21*, 266. [[CrossRef](#)]
29. Elsabee, M.Z.; Ali, E.A.; Mokhtar, S.M.; Eweis, M. Synthesis, characterization polymerization and antibacterial properties of novel thiophene substituted acrylamide. *React. Funct. Polym.* **2011**, *71*, 1187–1194. [[CrossRef](#)]
30. Hashmi, M.A.; Lein, M. Carbon nano-onions as photosensitizers: Stacking-induced red-shift. *J. Phys. Chem. C* **2018**, *122*, 2422–2431. [[CrossRef](#)]
31. Arshad, M.N.; Bibi, A.; Mahmood, T.; Asiri, A.M.; Ayub, K. Synthesis, crystal structures and spectroscopic properties of triazine-based hydrazone derivatives; A comparative experimental-theoretical study. *Molecules* **2015**, *20*, 5851–5874. [[CrossRef](#)] [[PubMed](#)]
32. Marder, S.R. Organic nonlinear optical materials: Where we have been and where we are going. *Chem. Commun.* **2006**, *37*, 131–134. [[CrossRef](#)]
33. Champagne, B.; Plaquet, A.; Pozzo, J.-L.; Rodriguez, V.; Castet, F. Nonlinear optical molecular switches as selective cation sensors. *J. Am. Chem. Soc.* **2012**, *134*, 8101–8103. [[CrossRef](#)]
34. Burland, D. Optical nonlinearities in chemistry: Introduction. *Chem. Rev.* **1994**, *94*, 1–2. [[CrossRef](#)]
35. Nayak, P.K.; Periasamy, N. Calculation of electron affinity, ionization potential, transport gap, optical band gap and exciton binding energy of organic solids using ‘solvation’ model and DFT. *Org. Electron.* **2009**, *10*, 1396–1400. [[CrossRef](#)]
36. Zhan, C.-G.; Nichols, J.A.; Dixon, D.A. Ionization potential, electron affinity, electronegativity, hardness, and electron excitation energy: Molecular properties from density functional theory orbital energies. *J. Phys. Chem. A* **2003**, *107*, 4184–4195. [[CrossRef](#)]
37. Frisch, M.J.; Trucks, G.W.; Schlegel, H.B.; Scuseria, G.E.; Robb, M.A.; Cheeseman, J.R.; Scalmani, G.; Barone, V.; Mennucci, B.; Petersson, G.A.; et al. *Gaussian 09 Revision D. 01*; Gaussian Inc.: Wallingford, CT, USA, 2010.
38. Adamo, C.; Barone, V. Toward reliable density functional methods without adjustable parameters: The PBE0 model. *J. Chem. Phys.* **1999**, *110*, 6158–6170. [[CrossRef](#)]
39. Perdew, J.P.; Burke, K.; Ernzerhof, M. Generalized gradient approximation made simple. *Phys. Rev. Lett.* **1996**, *77*, 3865–3868. [[CrossRef](#)]
40. Perdew, J.P.; Burke, K.; Ernzerhof, M. Generalized gradient approximation made simple. *Phys. Rev. Lett.* **1997**, *78*, 1396. [[CrossRef](#)]

41. Grimme, S. Semiempirical GGA-type density functional constructed with a long-range dispersion correction. *J. Comput. Chem.* **2006**, *27*, 1787–1799. [[CrossRef](#)]
42. Grimme, S.; Antony, J.; Ehrlich, S.; Krieg, H. A consistent and accurate ab initio parametrization of density functional dispersion correction (DFT-D) for the 94 elements H-Pu. *J. Chem. Phys.* **2010**, *132*, 154104. [[CrossRef](#)]
43. Grimme, S.; Ehrlich, S.; Goerigk, L. Effect of the damping function in dispersion corrected density functional theory. *J. Comput. Chem.* **2011**, *32*, 1456–1465. [[CrossRef](#)] [[PubMed](#)]
44. Weigend, F.; Ahlrichs, R. Balanced basis sets of split valence, triple zeta valence and quadruple zeta valence quality for H to Rn: Design and assessment of accuracy. *Phys. Chem. Chem. Phys.* **2005**, *7*, 3297–3305. [[CrossRef](#)] [[PubMed](#)]
45. Cammi, R.; Mennucci, B.; Tomasi, J. Fast evaluation of geometries and properties of excited molecules in solution: A Tamm-Dancoff Model with application to 4-dimethylaminobenzonitrile. *J. Phys. Chem. A* **2000**, *104*, 5631–5637. [[CrossRef](#)]
46. Cossi, M.; Barone, V. Solvent effect on vertical electronic transitions by the polarizable continuum model. *J. Chem. Phys.* **2000**, *112*, 2427–2435. [[CrossRef](#)]
47. Cossi, M.; Barone, V. Time-dependent density functional theory for molecules in liquid solutions. *J. Chem. Phys.* **2001**, *115*, 4708–4717. [[CrossRef](#)]
48. Cossi, M.; Rega, N.; Scalmani, G.; Barone, V. Polarizable dielectric model of solvation with inclusion of charge penetration effects. *J. Chem. Phys.* **2001**, *114*, 5691–5701. [[CrossRef](#)]
49. Cossi, M.; Scalmani, G.; Rega, N.; Barone, V. New developments in the polarizable continuum model for quantum mechanical and classical calculations on molecules in solution. *J. Chem. Phys.* **2002**, *117*, 43–54. [[CrossRef](#)]
50. Cossi, M.; Rega, N.; Scalmani, G.; Barone, V. Energies, structures, and electronic properties of molecules in solution with the C-PCM solvation model. *J. Comput. Chem.* **2003**, *24*, 669–681. [[CrossRef](#)]
51. Tomasi, J.; Mennucci, B.; Cammi, R. Quantum mechanical continuum solvation models. *Chem. Rev.* **2005**, *105*, 2999–3093. [[CrossRef](#)]
52. Marenich, A.V.; Cramer, C.J.; Truhlar, D.G. Universal solvation model based on solute electron density and on a continuum model of the solvent defined by the bulk dielectric constant and atomic surface tensions. *J. Phys. Chem. B* **2009**, *113*, 6378–6396. [[CrossRef](#)] [[PubMed](#)]
53. CYLview, B.; Legault, C.Y. Université de Sherbrooke. 2009. Available online: <http://www.cylview.org> (accessed on 12 January 2019).



© 2019 by the authors. Licensee MDPI, Basel, Switzerland. This article is an open access article distributed under the terms and conditions of the Creative Commons Attribution (CC BY) license (<http://creativecommons.org/licenses/by/4.0/>).